The Flexible, Polarizable, Thole-Type Interaction Potential for Water (TTM2-F) Revisited

George S. Fanourgakis and Sotiris S. Xantheas*

Chemical Sciences Division, Pacific Northwest National Laboratory, 902 Battelle Boulevard, PO Box 999, MS K1-83, Richland, Washington 99352

Received: November 9, 2005; In Final Form: January 18, 2006

We present a revision of the flexible, polarizable, Thole-type interaction potential for water [*J. Chem. Phys.* **2002**, *116*, 5115], which allows for condensed-phase simulations. The revised version (TTM2.1-F) of the potential correctly describes the individual water molecular dipole moment and alleviates problems arising at short intermolecular separations that can be sampled in the course of molecular dynamics and Monte Carlo simulations of condensed environments. Furthermore, its parallel implementation under periodic boundary conditions enables the efficient calculation of the macroscopic structural and thermodynamic properties of liquid water, as its performance scales superlinearly with up to a number of 64 processors for a simulation box of 512 molecules. We report the radial distribution functions, average energy, internal geometry, and dipole moment in the liquid as well as the density, dielectric constant, and self-diffusion coefficient at $T =$ 300 K from (*NVT*) and (*NPT*) classical molecular dynamics simulations by using the revised version of the potential.

I. Introduction

The main thrust behind the development of most interaction potentials for water is the study of the condensed phase such as liquid water and/or ice. This was clearly the intent behind the development of the Thole-type,[1] polarizable, rigid[2] (TTM2-R) and flexible[3] (TTM2-F) interaction potentials for water. The philosophy used in the parametrization of this class of potentials was based on the premise that a prerequisite for the accurate description of a many-body system (such as liquid water and/or ice) is the precise description of the few-body system (such as water clusters). To this end, water clusters were used as a means to assess the feasibility of describing the fundamental interactions at the molecular level and accounting for the collective effects. The accurate description of clusters represents quite a demanding test for an empirical potential because their structural and energetic features are the result of a delicate balance between the number of hydrogen/dangling bonds and the magnitude of the cooperative effects that are formed by the local networks. We have previously relied on the use of high-level ab initio results on water clusters[4,5] in order to assess the accuracy of the TTM2-R and TTM2-F potentials. In a recent study,[6] high-level ab initio calculations (establishing the complete basis set limit of the second-order Møller−Plesset perturbation theory) were performed for several isomers of the $(H_2O)_{20}$ cluster, and the results were compared with the predictions of several interaction potentials (AMOEBA,[7] TTM2-F,[3] TIP4P,[8] ASP-W4[9]), whose development has been based on different philosophies. One of the main conclusions of that study, in agreement with the findings of similar studies for clusters of smaller sizes,[4,5] is that the TTM2-F potential is able to reproduce the binding energies (D_e's) of these clusters quite accurately. More specifically, for several isomers belonging to the four main families of minima of $(H_2O)_{20}$ (dodecahedron, fused cubes, face-sharing pentagonal prisms, and edge-sharing pentagonal prisms), the binding energies predicted by the high-level ab initio methods and by the TTM2-F potential differ by $<1\%$, in better agreement than other empirical potentials, which reproduced the binding energies with an accuracy between 3 and 5% with respect to the ab initio results.

The TTM2-R and TTM2-F potentials were fitted to high-level electronic structure results for selected parts of the water dimer potential energy surface.[10] From Figure 1 of ref 2, it is seen that for inter-oxygen separations smaller than ∼2.5 Å, the total two-body energy decreases unrealistically as a result of the inverse (12−10−6) polynomial, which was used to describe the van der Waals and long-range pair potential. This behavior can be problematic in molecular dynamics (MD) or Monte Carlo (MC) simulations, during which these regions of the configuration space are sampled. The revisions of the potential that we introduce in the present study aim, not only in alleviating those problems so condensed-phase simulations become possible, but also facilitate their efficient execution via the parallelization of the evaluations of the energy and gradient of a periodic simulation box. Our intent was to introduce the minimum amount of changes into the functional form in an effort to keep the previously observed excellent agreement with cluster results intact. This is reflected in the naming scheme of the new potential (TTM2.1-F) indicating a revision (2.1) of the original (2.0) version of the potential and not a reparametrization. We reiterate that the present study aims in revising the flexible TTM2-F potential in a manner that makes liquid simulations feasible. In this paper, the results of classical simulations for liquid water with the revised version are presented in lieu of the fact that no liquid simulations with the original flexible version (TTM2-F) have been reported to date. Only short liquid simulations with the rigid version of the potential (TTM2-R) have been previously reported.[2] In the present study, we report the results of classical simulations despite the fact that it has been stated right from the beginning of the development of the model (see the end of the Introduction Section in ref 10) that

* To whom correspondence should be addressed. E-mail: sotiris.xantheas@pnl.gov.

10.1021/jp056477k CCC: $33.50
Published on Web 03/02/2006

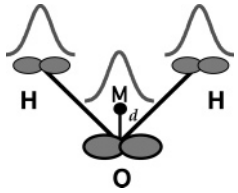

Figure 1. Thole-type model for water.

quantum (path integral) rather than classical simulations will be more appropriate in order to compare the results of macroscopic simulations using this potential with experiment because of the philosophy in its construction (fitted to D_e values and thus need explicit account for zero-point energy effects). In this way, the present study aims in establishing the reference data (results of classical simulations) used to quantify the importance of quantum effects and the direct comparison with experimental data in forthcoming studies.

In Section II, we discuss the revisions of the potential. In Section III, we outline the details of the molecular dynamics simulations and the parallelization of the code under periodic boundary conditions, which are used to simulate several macroscopic properties of liquid water. The results for water clusters and liquid water are presented and discussed in Section IV, whereas the conclusions of the present study are drawn in Section V.

II. The TTM2.1-F Interaction Potential

a. Overview of the TTM2-R and TTM2-F Potentials. The new version of the potential is based upon the rigid and flexible versions of the Thole-type model for water.[11] The rigid version[2] (TTM2-R) is an M-site model, having smeared induced dipoles on the atomic sites and smeared charges of 0.574 *e* on the hydrogen atoms and −1.148 *e* at a distance $d = 0.25$ Å away from the oxygen atom along the bisector of the HOH angle (M-site), as shown in Figure 1. The OH bond lengths are 0.9572 Å and the HOH angle 104.52°, resulting in a gas-phase molecular permanent dipole of 1.853 D. Thole's method[1] for expressing the dipole tensor in terms of the "reduced distance" $r_{ij}^{red} = r_{ij}/\tilde{A}$ was used, where $\tilde{A} = (\alpha_i\alpha_j)^{1/6}$ and α_i, α_j are the polarizabilities of atoms *i* and *j*, respectively. Among the many choices proposed by Thole[1] for the charge density, we used

$$\rho(r) = \frac{1}{\tilde{A}^3}\frac{3a}{4\pi}\exp\left(-a\left(\frac{r}{\tilde{A}}\right)^3\right) \tag{1}$$

in which *a* is the dimensionless width parameter that is parametrized for this density ($a^{CC} = a^{CD} = 0.2$ and $a^{DD} = 0.3$). CC denotes the charge−charge, CD the charge−dipole, and DD the dipole−dipole interactions, respectively. The only intramolecular contributions arise from the atomic (induced) dipole−dipole interactions. The induced dipoles on the O and H sites have polarizabilities of 0.837 Å^3 and 0.496 Å^3, respectively, producing a molecular polarizability of 1.433 Å^3 (experimental[12] value: 1.470 Å^3).

The total interaction for a system of *N* water molecules is written as

$$U_{tot} = U_{pair} + U_{elec} + U_{pol} \tag{2}$$

where

$$U_{pair} = \sum_{i=1}^{N-1}\sum_{j>i}^{N}\left(\frac{A}{r^{12}} + \frac{B}{r^{10}} + \frac{C}{r^6}\right) \tag{3}$$

$$U_{elec} = U_{CC} + U_{CD} + U_{DD} \tag{4}$$

$$U_{pol} = \sum_{i=1}^{K}\frac{\mu_i^2}{2\alpha_i} \tag{5}$$

are the pair (sums over the oxygen sites), electrostatic, and polarization components, respectively, μ_i is the induce dipole and α_i the polarizability of atomic site *i*, *K* is the total number of induced dipole sites ($K = 3N$). The coefficients *A*, *B*, and *C* were determined by fitting U_{tot} to symmetry-constrained energy curves[10] of the water dimer PES obtained at the second-order perturbation theory[13] (MP2) level with the aug-cc-pVTZ basis set[14] and uniformly scaled to the best estimate (at the complete basis set, MP2/CBS, limit) for the minimum geometry and energy.

The flexible version of the potential (TTM2-F) is based on the coupling of the Partridge−Schwenke (PS) water monomer potential energy (PES) and dipole moment (DMS) surfaces[15] to the intermolecular part via an intramolecular charge redistribution scheme, which accounts for the change of the static molecular dipole moment due to the change of the fragment's geometry. Because the molecular dipole derivative with respect to the elongation of the OH stretch does not lie along the nuclear displacement vector,[16] the term "nonlinear dipole moment surface" has been used. Partridge and Schwenke have produced a 245-term fit to the PES and an 84-term fit to the DMS from high-level ab initio calculations for the water monomer. The DMS is cast in terms of geometry-dependent charges according to

$$\begin{aligned}\mathbf{p}^g &= q(r_{H_1-O}, r_{H_2-O}, \theta_{HOH})\mathbf{r}_{H_1-O} + \\ &\qquad q(r_{H_2-O}, r_{H_1-O}, \theta_{HOH})\mathbf{r}_{H_2-O} \\ &= q^O\mathrm{r}_O + q^{H_1}\mathrm{r}_{H_1} + q^{H_2}\mathrm{r}_{H_2}\end{aligned} \tag{6}$$

where $\mathbf{p}^g$ is the gas-phase monomer dipole moment, $\mathbf{r}_{H_1-O} = \mathbf{r}_{H_1} - \mathbf{r}_O$, $\mathbf{r}_{H_2-O} = \mathbf{r}_{H_2} - \mathbf{r}_O$, $q(r_{H_1-O}, r_{H_2-O}, \theta_{HOH}) = q^{H_1}$, $q(r_{H_2-O}, r_{H_1-O}, \theta_{HOH}) = q^{H_2}$, and $q^O = -(q^{H_1} + q^{H_2})$. In other words, the partial charges *on the atomic* sites (H_1, H_2, O) are given as a function of the intramolecular geometry, viz. $q^a \equiv q^a(r_{H_1-O}, r_{H_2-O}, r_{H_1-H_2})$. Following the notation introduced in ref 3, superscripts indicate the charges on the atomic sites (H_1, H_2, O) provided by the Partridge−Schwenke DMS, whereas subscripts denote the partial charges on the charge sites (H_1, H_2, M-site) used in the model. At the gas-phase equilibrium geometry ($R_e = 0.9578$ Å, $\vartheta_e = 104.51°$) of the TTM2-F monomer, the charges on the atoms are 0.577 *e* (hydrogen) and −1.154 *e* (oxygen), as determined from the PS DMS (note that these are very close to the corresponding *fixed* charges of 0.574 *e* (H) and −1.148 *e* (O) for the TTM2-R model). The position along the bisector of the HOH angle of the massless "M-site", which carries the charge (instead of the oxygen atom) in the model, is determined via the holonomic constraint of Reimers et al.[17]

$$\mathrm{r}_M = \mathrm{r}_O + \frac{\gamma}{2}(\mathrm{r}_{H_1-O} + \mathrm{r}_{H_2-O}) \tag{7}$$

where $\gamma = 0.4267$. In the original TTM2-F potential, the partial

TABLE 1: Parameters of the Pairwise Additive Part[a]

parameters	TTM2-F	TTM2.1-F
A (Å^{12}·kcal/mol)	−1329565.985	
B (Å^{10}·kcal/mol)	363256.0798	
C (Å^{6}·kcal/mol)	−2147.141323	
D (kcal/mol)	0	1.0×10^{13}
E (Å^{-1})	0	13.2

[a] A, B, and C are common for the TTM2-F and TTM2.1-F potentials.

charges q_a on the charge-bearing sites were chosen from the q^a coefficients (which are the charges on the nuclear sites obtained from the PS DMS) according to the relations:

$$q_{H_1} = \frac{q^{H_1}}{(1-\gamma)}$$
$$q_{H_2} = \frac{q^{H_2}}{(1-\gamma)} \qquad (8)$$
$$q_M = -(q_{H_1} + q_{H_2})$$

This choice of partial charges, which was made in the original TTM2-F version, results in a monomer dipole moment $\tilde{\mathbf{p}}^g$, which differs from the one obtained from the PS DMS, $\mathbf{p}^g$, by:

$$\tilde{\mathbf{p}}^g = q_M \mathbf{r}_M + q_{H_1}\mathbf{r}_{H_1} + q_{H_2}\mathbf{r}_{H_2}$$
$$= \mathbf{p}^g + \frac{\gamma}{2(1-\gamma)}(q^{H_1} - q^{H_2})(\mathrm{r}_{H_1} - \mathrm{r}_{H_2}) \qquad (9)$$

Hence the DMS of the water monomer is not properly described when the choice of charges in eq 8 is used. The revisions of the potential to correct this problem are discussed below.

b. Revised Pairwise Additive Term. The inverse (12−10−6) polynomial, which describes the long-range van der Waals interactions between the oxygen atoms as well as the repulsive interactions at short O−O separations, has been modified to include an additional exponential term according to

$$V(r) = \frac{A}{r^{12}} + \frac{B}{r^{10}} + \frac{C}{r^6} + De^{-Er} \qquad (10)$$

where r stands for the intermolecular O−O separation. As noted earlier, the reason behind this modification is that, in the original form, the energy decreases unrealistically at short distances, which are sampled during condensed-phase simulations. We have found that, in several cases during either molecular dynamics or Monte Carlo simulations, the system is trapped in that region. The parameters A, B, C, D, and E for both potentials are given in Table 1. Given our intention, as stated in the Introduction, to introduce only minor changes into the functional form, and as a result, a minor revision rather than a reparametrization of the potential, the coefficients A, B, and C were kept the same as in the original TTM2-F version, while the parameters D and E of the exponential were chosen in such a way that they affect the energy only at short distances for which it now has the expected physical behavior. This is shown schematically in Figure 2. The revised (TTM2.1-F) pairwise additive term is indicated with a solid line, whereas the original (TTM2-F) term is indicated with a dashed line in Figure 2.

c. Partial Charges. In the revised version (TTM2.1-F), the charges q_a on the charge-bearing sites (H_1, H_2, M) are determined from the charges q^a on the nuclear sites (which are taken from the PS DMS) according to

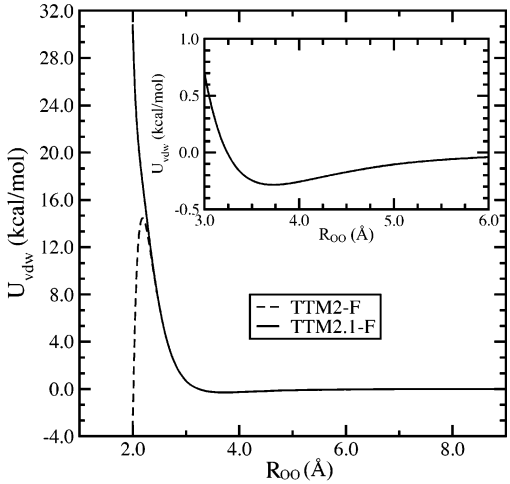

Figure 2. Pairwise additive part for the O−O interaction for the TTM2.1-F (solid line) and the TTM2-F (dashed line) potentials. The two potential forms differ only in the short range, while at larger separations, the inner graph clearly shows that the two potentials coincide.

$$q_{H_1} = q^{H_1} - \frac{\gamma}{2(1-\gamma)}q^O$$
$$q_{H_2} = q^{H_2} - \frac{\gamma}{2(1-\gamma)}q^O \qquad (11)$$
$$q_M = -(q_{H_1} + q_{H_2}) = \frac{q^O}{1-\gamma}$$

These choices satisfy the neutrality constraint, viz. $q_{H_1} + q_{H_2} + q_M = q^{H_1} + q^{H_2} + q^O = 0$, and furthermore, when substituted into eq 6, yield the correct dipole moment predicted by the PS DMS, viz. $\mathbf{p}^g = q_M\mathbf{r}_M + q_{H_1}\mathbf{r}_{H_1} + q_{H_2}\mathbf{r}_{H_2} = q^O\mathbf{r}_O + q^{H_1}\mathbf{r}_{H_1} + q^{H_2}\mathbf{r}_{H_2}$.

It is noted that the set of new charges for the revised TTM2.1-F potential (eq 11) reverts to the set of charges for the original TTM2-F version (eq 8) for configurations having C_{2v} symmetry, for which $q_{H_1} = q_{H_2} = q_H = -q_O/2$. To a first approximation, the energetic differences between the two versions of the potential will be proportional to the degree of distortion of the constituent fragments away from C_{2v} symmetry (asymmetry of OH bonds). The effect of the choice of new partial charges on the cluster energies will be discussed in Section IV.

III. Computational Details

a. Molecular Dynamics Simulations. Classical molecular dynamics (MD) simulations were carried out under constant density and temperature (*NVT* ensemble), and under constant pressure and temperature (*NPT* ensemble) conditions, by implementing the Nose−Hoover thermostat[18] and the Berendsen barostat,[19] respectively. During all simulations, a cubic box containing 256 water molecules was used, and periodic boundary conditions were imposed. For the van der Waals interactions, a spherical cutoff of $R_c = 9.0$ Å was assumed, and the standard long-range corrections[20] for the energy and the pressure were applied. For the electrostatic interactions, the standard Ewald summation technique was adopted (implemented as it is described in ref 21). In the real space, we considered all interactions between charges and dipoles inside the simulation box, while in the reciprocal space, 2×873 k-points were used.

The Ewald parameter has a value $\kappa = 0.3$ Å^{-1}. The velocity-Verlet algorithm[22] was used to propagate the MD trajectory for 1 ns. A time step of 0.2 fs was employed in order to ensure accurate sampling of the high-frequency OH stretching vibrations. The first 200 ps were used as an equilibration period, and they were not taken into account in the calculation of average properties. Statistical errors of average quantities were estimated by using block averages.

The amount of computational time needed for the evaluation of the energy and force of a polarizable model is usually significantly larger in comparison to a pairwise additive one due to the calculation of the induced dipole moments. By using a self-consistent iterative procedure at every time step, the induced dipoles on the hydrogen atoms and the M-site converged to a (rms) threshold of 10^{-6} Debye. The number of iterations required depends on the initial guess of the induced dipoles. This is usually achieved in 3−4 iterations when using the extrapolation scheme of Ahlström et al.[23] In an attempt to further reduce the simulation time, the code was parallelized and executed in a computer cluster using 32 processors. A few details of the algorithms and the performance of the codes are given in the subsequent section, while the full details of the parallelization effort will be described in a future work.[24]

The diffusion coefficient was estimated from the mean-square displacement formula[20]

$$D = \frac{1}{6}\frac{\mathrm{d}}{\mathrm{d}t}\langle|\mathbf{r}(t) - \mathbf{r}(t_0)|^2\rangle \tag{12}$$

which holds in the long time limit. For molecular systems, this relation can be applied to any atom. For the estimation of the static dielectric constant, we used[25]

$$\epsilon_0 = 1 + \frac{4\pi}{3k_{\mathrm{B}}TV}(\langle\mathbf{M}^2\rangle - \langle\mathbf{M}\rangle\cdot\langle\mathbf{M}\rangle) \tag{13}$$

where **M** is the total dipole moment of the simulation box.

b. Parallelization Protocol and Scaling under Periodic Boundary Conditions. For the evaluation of the energy and the forces of the TTM2.1-F potential under periodic boundary conditions used during the MD simulations, a parallel code in FORTRAN-90 has been developed. The performance of the code has been examined in a cluster of 64 Itanium 2 processors running Linux and using INTEL's efc compiler. A few technical details are given here, while the complete algorithm will be described elsewhere.[24]

In the real space, the total number of interactions (both van der Waals and electrostatic) between the atoms is divided in small blocks, and each processor calculates a partial sum of the energies and the forces. In the same manner, the *k*-points have been equally distributed among the processors, and each of them performs a partial sum in the reciprocal space. For the calculation of the induced dipoles, evaluations of a matrix−vector multiplication between the dipole moment tensor $\boldsymbol{A}$ and the electric field $\boldsymbol{E}_f$ are required. The number of the multiplications depends on the initial guess of the electric field and the accuracy of the induced dipoles as required by the convergence criterion. In our implementation, we have divided the ($9N \times 9N$) dipole moment tensor in p^2 subarrays of size ($n \times n$), where $n = 9N/p$, and p is the number of processors. Each processor calculates the matrix elements of p subarrays and performs p matrix−vector multiplications of size $(n \times n) \times n$. Given the fact that the dipole moment tensor $\boldsymbol{A}$ is symmetric, each subarray and its symmetric counterpart is distributed in the same processor, avoiding in this way the recalculation of the same matrix elements in another processor or data transfer from one processor to another. At the end of this step, each processor contains a vector of size $9N$, which is broadcasted to the other processors. The global sum of these vectors is the new electric field, which is used for the next iteration until the required accuracy is achieved. The remaining terms in the energy expression (eqs 2−5) and the forces involving the dipole moment are evaluated in parallel by dividing again the total number of interactions in small blocks.

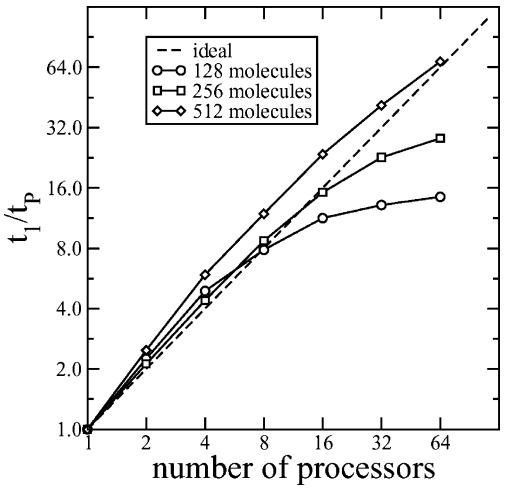

Figure 3. Scaling of the parallel version of the TTM2.1-F potential with number of processors p for different sizes of the simulation box. See also eq 14 in the text.

The scaling of the above algorithm was evaluated by performing MD simulations with periodic boundary conditions of 1000 time steps for three simulation boxes containing $N =$ 128, 256, and 512 water molecules, respectively. The corresponding size $9N$ dipole−tensor array is 1152, 2304, and 4608 for the three simulation boxes, respectively. For the initial guess of the electric field required for the calculation of the dipole moment, the extrapolation scheme of Ahlström et al.[23] was employed. The scaling of the code for the three different simulation boxes is shown in Figure 3 for $p = 1-64$ processors. The speed-up (s) with respect to the serial wall time t_1 is defined as

$$s = \frac{1}{p}\left(\frac{t_1}{t_p}\right) \tag{14}$$

where t_{p} is the corresponding execution time on p processors.

The performance of the parallel code exhibits the following common characteristics for all three simulation boxes: a superlinear scaling, a point of linear scaling, and from then on a sublinear scaling with the number of processors. The superlinear scaling is mainly the result of the part of the code that performs matrix−vector multiplications during the iterative process, which determines the induced dipoles. Although some communication between processors is involved, the smaller sizes of matrix−vector multiplications can be performed inside the cache of each processor, resulting in this way in an overall better performance. The reason that for a given system size the scaling drops with the number of processors is because, after some point, there is not "enough work" to be distributed among the processors and the communication time becomes significant. For the simulation boxes of 128, 256 and 512 molecules, the optimum number of processors that show linear scaling is 8, 16 and 64, respectively. This efficient scaling of the parallel version of the code allows for longer simulations, the treatment

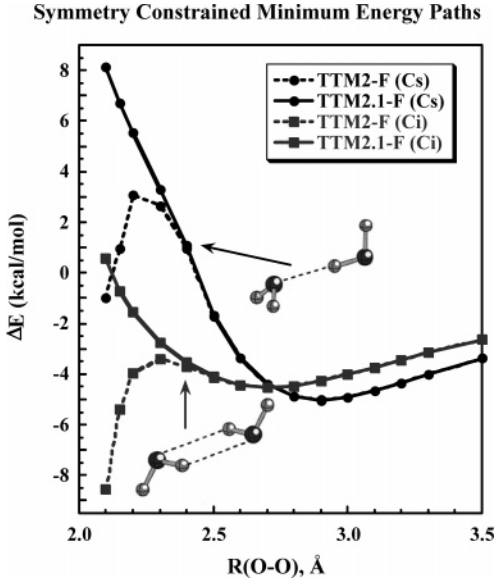

Figure 4. Symmetry-constrained minimum energy curves for the water dimer as a function of the O−O separation under C_s (circles) and C_i (diamonds) symmetry with the TTM2.1-F (solid line) and TTM2-F (dashed line) potentials.

of larger simulation cells, and shorter time-to-solution. To the best of our knowledge, this is the first reported result for the scaling of a *polarizable* potential for water under periodic boundary conditions during MD simulations.

IV. Results and Discussion

a. Water Dimer Symmetry-Constrained Minimum Energy Paths. The symmetry-constrained minimum energy paths (MEPs) for the water dimer are shown in Figure 4 with the TTM2.1-F (solid lines) and TTM2-F (dashed lines) potentials. The MEPs along the C_s (circles) and C_i (squares) symmetries are shown. Those for the TTM2-F potential have not been published before, but they appear similar to the ones previously reported[2] for the (rigid) TTM2-R potential, in that the MEP for the C_i symmetry behaves unrealistically for R(O−O) < 2.3 Å. We further note that the MEP along the C_s symmetry with the TTM2-F potential also behaves unrealistically at the same range of the interoxygen separation. In contrast, the TTM2.1-F potential does show the expected physical behavior in the repulsive wall of the potential. This is due to the use of the enhanced pair-additive term (eq 10), which affects only the repulsive wall while it has practically no effect for R(O−O) > 2.4 Å.

b. Water Clusters. Because the water cluster binding energies were previously used as means to assess the accuracy of the TTM2-F potential, it is of interest to investigate whether the proposed revisions affect the excellent agreement that was previously found between the TTM2-F and the MP2/CBS binding energies. The binding energies with the TTM2-F and TTM2.1-F potentials, together with the ones obtained[4−6] at the MP2/CBS level for the $(H_2O)_n$, $n = 2-6$, 8, and 20, are listed in Table 2. The proposed revisions affect the dimer binding energy by <0.01 kcal/mol, whereas even up to $n = 20$ the changes are minimal, <0.25 kcal/mol. The differences between the TTM2-F and TTM2.1-F potentials are negligible, as they amount to a maximum difference of 0.3%, whereas for all 4 isomers of $n = 20$, they are ∼0.1%. Therefore, the excellent agreement of the TTM2.1-F potential with the MP2/CBS binding energies of water clusters is maintained under the proposed revisions.

TABLE 2: Binding Energies of Water Clusters $(H_2O)_n$, $n = 2-6$, 8, 20, with the TTM2-F and TTM2.1-F Potentials[a]

cluster size (n)	TTM2-F	TTM2.1-F	MP2/CBS
2	−5.02	−5.03	−4.98
3	−15.90	−15.94	−15.8
4	−27.55	−27.63	−27.6
5	−36.69	−36.81	−36.3
6 cage	−46.44	−46.51	−45.8
6 ring	−45.03	−45.17	−44.8
6 prism	−45.86	−45.91	−45.9
6 book	−45.99	−46.09	−45.6
8 (S_4)	−73.24	−73.33	−72.7
20 dodecahedron	−202.22	−202.48	−200.1
20 fused cubes	−214.29	−214.35	−212.6
20 face-sharing pentagonal prisms	−213.98	−214.08	−215.0
20 edge-sharing pentagonal prisms	−216.34	−216.46	−217.9

[a] The MP2/CBS values are also listed for comparison.

The changes in the cluster structures upon the proposed revisions also appear to be insignificant. Previous ab initio calculations[3,4] have shown that the bend angle of the constituent water molecules increases with respect to the isolated monomer with cluster size. It has been previously[3] emphasized that only by the use of the nonlinear DMS of the water monomer was the TTM2-F potential able to reproduce this trend accurately. Because this remains the same in TTM2.1-F, albeit by a different choice of the partial charges as outlined in Section II.c., we expect this trend to hold with the TTM2.1-F potential. The results for the average HOH angle increase, $\langle \Delta \vartheta_{HOH} \rangle$, and hydrogen-bonded OH stretch increase, $\langle \Delta r_{HO}{}^b \rangle$, for clusters $n = 2-6$ with the TTM2-F and TTM2.1-F potentials, are listed in Table 3, together with the corresponding results obtained at the MP2 level of theory with the aug-cc-pVTZ basis set. The TTM2.1-F potential produces average angle increases within <0.01° and average hydrogen-bonded OH stretch increases that are <0.001 Å from the corresponding TTM2-F values. Therefore, the relative error with respect to the ab initio results is of the same magnitude with the TTM2.1-F and TTM2-F potentials. It should be noted that the values of Table 3 for the angles and bond lengths with the TTM2-F potential are slightly different from the ones reported in an earlier study,[3] as much more stringent geometry convergence criteria were used in the present study in order to obtain the minimum cluster geometries. The results of this section suggest that the proposed changes in the van der Waals and the choice of partial charges (eq 11), which were dictated to correct previous inconsistencies, have a negligible effect on the structural and energetic properties of water clusters up to $n = 21$.

c. Liquid Water. The (*NVT*) simulation at room temperature (300 K) and at experimental density ($\rho = 0.997$ g/cm^3) yielded an average pressure of $P = -1800 \pm 385$ atm. The average potential energy is estimated at $E_{liq} = -10.78 \pm 0.02$kcal/mol. An additional simulation for the gas-phase water monomer at the same temperature yielded $E_{gas} = 0.90$kcal/mol. The heat of vaporization is given by:

$$\Delta H_v = -\Delta E + \Delta PV = -E_{liq} + E_{gas} + k_B T \qquad (15)$$

where $k_B T = 0.59$ kcal/mol. This leads to an estimation of $\Delta H_v = 12.27 \pm 0.02$ kcal/mol for the heat of vaporization with the TTM2.1-F potential, a value that differs significantly from the experimental one of 10.51 kcal/mol.[8,26] We will discuss this "deviation" in the context of the simulation methods that are appropriate to estimate this quantity in a manner consistent with the philosophy behind the original parametrization of the potential in the subsequent section.

TABLE 3: Changes in the Internal Geometry of Water with Respect to the Gas-Phase Monomer for the Dimer and the Cyclic Structures of Water Clusters $n = 3-6$[a]

	$\langle\Delta\vartheta_{HOH}\rangle$			$\langle\Delta r_{HO}{}^{b}\rangle$			$\langle\Delta r_{HO}{}^{0}\rangle$		
n	TTM2-F	TTM2.1-F	MP2	TTM2-F	TTM2.1-F	MP2	TTM2-F	TTM2.1-F	MP2
2	0.436	0.435	0.400	0.0073	0.0081	0.0072	−0.0004	−0.0006	−0.0010
3	1.225	1.219	1.323	0.0125	0.0133	0.0131	−0.0027	−0.0034	−0.0006
4	1.371	1.362	1.239	0.0128	0.0140	0.0213	−0.0029	−0.0039	−0.0005
5	1.323	1.311	1.107	0.0125	0.0138	0.0221	−0.0030	−0.0042	−0.0005
6	1.249	1.236	0.982	0.0122	0.0135	0.0222	−0.0029	−0.0041	−0.0008

[a] $\langle\Delta\vartheta_{HOH}\rangle$ denotes the average change of the bend angle, whereas $\langle\Delta r_{HO}\rangle$ denotes the change of the average OH bonds. The superscripts "b" and "0" refer to the hydrogen bonded and "free" OH stretches, respectively. The MP2 results are obtained with the aug-cc-pVTZ basis set.

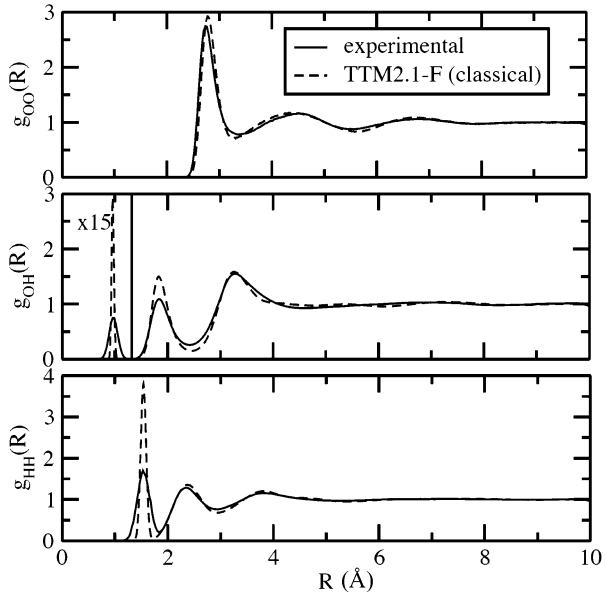

Figure 5. Radial distribution functions for O−O, O−H, and H−H from molecular dynamics simulations of liquid water at $T = 300$ K and $\rho = 0.997$ g/cm^3. Dashed line: TTM2.1-F potential; solid line: neutron scattering experiment. The intramolecular OH (less than the cutoff value of <1.2 Å, which is denoted by a vertical line) has been scaled by a factor of 15.

For the dielectric constant, we obtain a value of $\epsilon_0 = 67.2$ (experimental value:[27] 78.3), and for the self-diffusion coefficient, a value of $D = 1.4 \times 10^{-5}$ cm^2/s (experimental value: [28] 2.3×10^{-5} cm^2/s). Finally, we obtain an average molecular dipole moment of 2.67 D.

The large negative value of pressure found in the MD simulation implies that the TTM2.1-F model should predict a value for the liquid density at $P = 1$ atm and $T = 298.15$ K, which is higher than the experimental one. The (*NPT*) simulation at these conditions yielded $\rho = 1.046 \pm 0.001$ g/cm^3 and $\Delta H_v = 12.07 \pm 0.02$ kcal/mol. This value for the density coincides with the one estimated for the rigid version[2] of the potential (TTM2-R), while the value for the heat of vaporization is even larger than the corresponding one for the rigid version (11.8 kcal/mol).

The radial distribution functions (RDFs) from the *NVT* simulation are shown in Figure 5, together with the ones obtained from neutron scattering experiments by Soper.[29] It is readily seen that there is an overall good agreement for the $g_{OO}(R)$, both in the position as well as the height of the first and second peaks. The first peak appears at 2.78 Å, which is 0.05 Å larger than the experimental one (2.73 Å). For the second peak, the calculated location is smaller by ∼0.1 Å than the experimental one. For the $g_{OH}(R)$ and $g_{HH}(R)$ RDFs, while the position of the peaks are close to the experimental ones, the heights of the peaks are significantly different. The first peak of both curves corresponding to the intramolecular O−H and H−H separations is also much narrower when compared to experiment. As a result, the calculated heights of the O−H and H−H first peaks are ∼4 and ∼2 times larger than the experimental ones, suggesting that the amplitude of the intramolecular vibrations is much smaller. For the intermolecular O···O and O···H separations, the experimental and calculated distributions are much closer.

Furthermore, the TTM2.1-F potential correctly predicts the trend of the increase of the intramolecular HOH angle in the liquid phase with respect to the gas-phase value. Experimentally, it has been suggested that the intramolecular bend increases from 104.5° for the gas-phase monomer[30] to 106.1 ± 1.8° for the liquid.[31] For the TTM2.1-F potential, this increase is identical: the average angle increases from 104.5° (gas phase) to 106.3° (liquid). To the best of our knowledge, TTM2.1-F is the *only* flexible interaction potential for water that correctly describes this trend, while all other empirical flexible potentials producing the opposite trend, i.e., a decrease of the angle in the liquid from the gas-phase value. The reason for this behavior has been attributed to the use of the monomer nonlinear dipole moment surface, i.e., the geometrical dependence of the charges as outlined in our previous work,[3] whereas all other empirical potentials are based on a linear monomer DMS. It should be mentioned that two recently developed models, which are also based on Thole's method but they employ constant charges (AMOEBA,[7] AMOEBA-v[32]), both predict a dramatic decrease of the intramolecular angle from the gas phase to the liquid. For AMOEBA, the bend angle decreases from 108.5° (gas phase) to 105.3° (liquid), whereas for AMOEBA-v, it decreases from 104.5° (gas phase) to 101° (liquid).

Finally, the TTM2.1-F potential predicts the average OH bond length in the liquid to be 0.968 Å, an increase of 0.011 Å from the gas-phase value of 0.957 Å, in good agreement with the experimental estimate of 0.970 Å.[31]

V. Conclusions and Outlook

In this study, we presented a revision of the flexible, polarizable empirical potential for water (TTM2.1-F), which treats the molecular dipole moment in a manner consistent with the PS DMS and corrects the unphysical behavior of the previous version in the region of the repulsive well. These revisions have a negligible effect on the structures and binding energies of water clusters up to $n = 20$ with respect to the original version (TTM2-F). It should be mentioned that, in several previous studies, we have shown that the cluster binding energies with the TTM2-F potential are in excellent agreement with the results of high-level ab initio (MP2/CBS) calculations. This agreement of the cluster energetics is maintained with the revised (TTM2.1-F) version. A parallel implementation of the TTM2.1-F potential under periodic boundary conditions results in a superlinear scaling with a number of processors for

simulation cells that are appropriate for statistical sampling (up to 512 water molecules).

The classical molecular dynamics simulations of macroscopic properties of liquid water with the TTM2.1-F potential produced qualitative agreement of the radial distribution functions, diffusion coefficient, and dielectric constant with respect to experiment, although the height of the peaks of the radial distribution functions (especially the intramolecular O−H and H−H) differ significantly from the experimental ones. Furthermore, at standard conditions ($T = 300$ K, $P = 1$ atm), the predicted heat of vaporization is by ∼1.7 kcal/mol larger and the density ∼5% higher than the experimental values.

The results mentioned above may imply limitations of the TTM2.1-F potential to describe the liquid phase of water; however, we believe that, for a fair comparison of the predictions of the model with the experiment, the inclusion of quantum effects should be considered. This is especially the case for the TTM2.1-F model, which was fitted to the bottom of the potential well (D_e) of clusters, suggesting that zero-point effects should *explicitly* be taken into account in order to derive macroscopic thermodynamic observables. Previous path integral molecular dynamics (PIMD) and path integral Monte Carlo (PIMC) simulations, performed for several water models, have demonstrated the importance of the quantum effects at room temperature.

Stern and Berne[33] have used the flexible, polarizable MCDHO water potential in constant temperature PIMD simulations with a simulation cell of 125 water molecules. At $T = 298.15$ K and $\rho = 0.997$ g/cm^3, they found that the energy difference $E_{liq} - E_{gas}$ is ∼1.5 kcal/mol larger than the one obtained from classical MD simulations. Mahoney and Jorgensen[34] have used a modified flexible version of the TIP4P model (called TIP4F) in which the flexibility of the water model was modeled by using harmonic oscillators. In their simulations, they used a system of 125 water molecules, and they compared the classical and quantum predictions over a range of temperatures and pressures using PIMC in the isothermal−isobaric ensemble. At $T = 298$ K and $P = 1$ atm, the simulations predicted $E_{liq} - E_{gas} = 12.365$ kcal/mol (classical) and 9.747 kcal/mol (quantum), respectively (difference 2.6 kcal/mol), and densities $\rho = 0.9948$ g/cm^3 (classical) and 0.9236 g/cm^3 (quantum), respectively (∼7% change). The results of these studies can offer an estimate of the size of the quantum corrections on the heat of vaporization and density. Both studies suggest that the heat of vaporization and the density will both decrease upon the introduction of quantum corrections. If these corrections are of the same magnitude for the TTM2.1-F potential, this will result in a better agreement of the results for the heat of vaporization and density with respect to experiment. Quantum effects will also affect (increase) the self-diffusion coefficient by a factor[35] of about 1.8 due to the lowering of the corresponding barriers for diffusion; this effect can account for the low value of the diffusion coefficient with respect to the experimental value obtained during classical MD simulations in this study. Because of the complexity of the TTM2.1-F potential, such simulations are currently prohibitive without an efficient parallelization of the quantum calculations, which can decrease the required computational time by at least an additional order of magnitude. We are currently working on extending the parallelization of the classical simulations, presented in this study, to include the quantum (PIMC) simulations in order to address the magnitude of the quantum corrections for the TTM2.1-F potential in forthcoming studies.

A Fortran-90 subroutine with the new version of the TTM2.1-F potential can be downloaded from http://www.pnl.gov/chemistry/highlights/water_potential.htm.

Acknowledgment. We wish to thank Drs. E. Aprà, M. Krishnan, and V. Tipparaju for helpful discussions during the development of the parallel code and Dr. Gregory Schenter for helpful discussions. This work was supported by the Division of Chemical Sciences, Office of Basic Energy Sciences, U.S. Department of Energy. Battelle operates the Pacific Northwest National Laboratory for the Department of Energy. This research was performed in part by using the Molecular Science Computing Facility (MSCF) in the William R. Wiley Environmental Molecular Sciences Laboratory, a national scientific user facility sponsored by the Department of Energy's Office of Biological and Environmental Research and located at Pacific Northwest National Laboratory.

References and Notes

(1) Thole, B. T. *Chem. Phys*. **1981**, *59*, 341.
(2) Burnham, C. J.; Xantheas, S. S. *J. Chem. Phys.* **2002**, *116*, 1500.
(3) Burnham, C. J.; Xantheas, S. S. *J. Chem. Phys.* **2002**, *116*, 5115.
(4) Xantheas, S. S.; Burnham, C. J.; Harrison, R. J. *J. Chem. Phys.* **2002**, *116*, 1493.
(5) Xantheas, S. S.; Aprà, E. *J. Chem. Phys.* **2004**, *120*, 823.
(6) Fanourgakis, G. S.; Aprà, E.; Xantheas, S. S. *J. Chem. Phys.* **2004**, *121*, 2655.
(7) Ren, P.; Ponder, J. W. *J. Phys. Chem. B* **2003**, *107*, 5933.
(8) Jorgensen, W. L.; Chandrasekhar, J.; Madura, J. D.; Impey, R. W.; Klein, M. L. *J. Chem. Phys.* **1983**, *79*, 926.
(9) Millot, C.; Soetens, J.-C.; Martins Costa, M. T. C.; Hodges, M. P.; Stone, A. J. *J. Phys. Chem. A* **1998**, *102*, 754.
(10) Burnham, C. J.; Xantheas, S. S. *J. Chem. Phys.* **2002**, *116*, 1479.
(11) Burnham, C. J.; Li, J.; Xantheas, S. S.; Leslie, M. *J. Chem. Phys.* **1999**, *110*, 4566.
(12) Murphy, W. F. *J. Chem. Phys.* **1977**, *67*, 5877.
(13) Møller, C.; Plesset, M. S. *Phys. Rev.* **1934**, *46*, 618.
(14) Dunning, T. H., Jr. *J. Chem. Phys.* **1989**, *90*, 1007. Kendall, R. A.; Dunning, T. H., Jr.; Harrison, R. J. *J. Chem. Phys.* **1992**, *96*, 6796.
(15) Partridge, H.; Schwenke, D. W. *J. Chem. Phys*. **1997**, *106*, 4618.
(16) Ikawa, S.-I.; Maeda, S. *Spectrochim. Acta*, *Part A* **1968**, *24*, 655. Whalley, E.; Klug, D. D. *J. Chem. Phys*. **1986**, *84*, 78.
(17) Reimers, J. R.; Watts, R. O.; Klein, M. L. *Chem. Phys*. **1982**, *64*, 95. Reimers, J. R.; Watts, R. O. *Chem. Phys*. **1984**, *85*, 83. Suhm, M. A.; Watts, R. O. *Mol. Phys*. **1991**, *73*, 463.
(18) Nosé, S. *Mol. Phys.* **1984**, *52*, 255.
(19) Berendsen, H. J. C.; Postma, J. P. M.; van Gunsteren, W. F.; DiNola, A.; Haak, J. R. *J. Chem. Phys*. **1984**, *81*, 3684.
(20) Allen, M. P.; Tildesley, D. J. *Computer Simulations of Liquids*; Oxford University Press: Oxford, 1987.
(21) Nymand, T. M.; Linse, P. *J. Chem. Phys*. **2000**, *112*, 6152.
(22) Swope, W. C.; Andersen, H. C.; Berens, P. H.; Wilson, K. R. *J. Chem. Phys*. **1982**, *76*, 637.
(23) Ahlström, P.; Wallqvist, A.; Engstrom, S.; Jonsson, B. *Mol. Phys*. **1989**, *68*, 563.
(24) Fanourgakis, G. S.; Tipparaju, V.; Nieplocha, J.; Xantheas, S. S. Work in progress.
(25) Neumann, M.; Steinhauser, O. *Chem. Phys. Lett.* **1984**, *106*, 563.
(26) Kell, G. S. *J. Chem. Eng. Data* **1975**, *20*, 97. Dorsey, N. E. *Properties of Ordinary Water-Substance*; ACS Monograph Series; Reinhold: New York, 1940; p 616.
(27) Bertolini, D.; Cassettari, M.; Salvetti, G. *J. Chem. Phys*. **1982**, *76*, 3285. Buchner, R.; Barthel, J.; Stauber, J. *Chem. Phys. Lett.* **1999**, *306*, 57.
(28) Krynicki, K.; Green, C. D.; Sawyer, D. W. *Discuss. Faraday Soc*. **1978**, *66*, 199.
(29) Soper, A. K. *Chem. Phys.* **2000**, *258*, 121.
(30) Benedict, W. S.; Gailar, N.; Plyler, E. K. *J. Chem. Phys*. **1956**, *24*, 1139.
(31) Ichikawa, K.; Kameda, Y.; Yamaguchi, T.; Wakita, H.; Misawa, M. *Mol. Phys.* **1991**, *73*, 79.
(32) Ren, P.; Ponder, J. W. *J. Phys. Chem. B* **2004**, *108*, 13427.
(33) Stern, H. A.; Berne, B. J. *J. Chem. Phys.* **2001**, *115*, 7622.
(34) Mahoney, M. W.; Jorgensen, W. L. *J. Chem. Phys.* **2001**, *115*, 10758.
(35) Poulsen, J. A.; Nyman, G.; Rossky, P. J. *Proc. Natl. Acad. Sci. U.S.A.* **2005**, *102*, 6709.